

LASER BEAM SCANNING FOR 3D MEASUREMENT PURPOSES

Abstract: A 3D range sensor is presented. The sensor is based on the relationship between a camera and a scanning laser beam. Triangulation is used to reconstruct the scene by using the information on the image plane of the camera and the angular position of the laser plane. Camera and laser modelling and calibrating have been studied and validated. The system has been implemented and some experimental results are shown in the paper.

1 Introduction

3D Measurement is still being a great challenge. Although lot of research is involved in stereovision systems (Barnard and Fischler 1982), most of the geometrical problems can be reduced when the system is used in industrial applications (Besl 1988). Moreover, light control can be achieved allowing better segmentation results. The Robotics and Computer Vision Group at the University of Girona is involved in 3D Measurement developing systems for either research willing and industrial applications. In this way, the group has developed a laser range sensor for 3D measurement purposes (Jarvis 1983).

The paper will present a computer vision system and a slit laser beam whose have been integrated in order to build up a full operatively 3D measurement system, see figure 1. The laser beam rotates by means of a DC motor in order to scan the whole camera scope getting a reconstruction of the scene. The power control card has been adapted to the new drivers technology and integrates the supply, the motor PWM control and the incremental encoder used to obtain the angular position of the laser beam. Furthermore, a processing card has been used in order to segment the image and obtain the 2D co-ordinates of the laser beam in the image plane at video rate. The processing card converts the space colour from RGB to HLS and segment the laser light from the rest of the scene by using LUT memories. Then, the card processes the video lines with the aim of obtaining the 2D co-ordinates. The first co-ordinate is given by the video line explored by the card, the second co-ordinate is given by computing the gravity centre of the segmented pixels. The card also synchronises the camera with the laser and gets the angular position of it for each image shot. Once the whole image is processed the information is sent to the computer which gets the 3D reconstruction. A window-based application has been built up in order to control the full system. The 3D sensor can be used for several industrial applications. Moreover, a green laser beam has been chosen instead of a red one getting better segmentation results under no light controlled scenarios. Then, the system is useful for robotic applications like indoor/outdoor navigation. In this way, we are still working on adapting the system to measure undersea scenes with the aim of improving our underwater robot capabilities (Jaffe 1990).

The paper is structured as follows. Firstly, camera and laser beam modelling and calibrating is explain in section 2. Moreover, section 3 includes the principle we have used to reconstruct the scene. Section 4 presents the structure of the sensor and the video rate card we have used for image processing and laser beam control. Section 5 presents the system validation and, finally, section 6 shows the experimental results. The paper ends with the conclusions and further work.

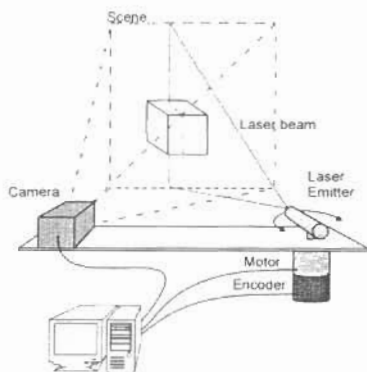


Figure 1 The proposed 3D scanning system.

2 System Modelling and Calibrating

This section deals with the studying of the mathematical model of the camera and the rotating laser. Then, the physical and spatial parameters of the both elements are obtained by calibration. Once the system is calibrated it can be used for 3D reconstruction (Salvi 1997).

2.1 Camera Modelling

The pinhole model is based on the reducing the camera behaviour complexity to an image plane I where the scene is projected through the focal point O_C . The focal point is placed at a fixed distance f from the image plane and no lens distortion is included. Then, giving a 3D object point P its 2D image projection p is obtained by intersection the optical ray v defined by P and O_C and the image plane I . This model is defined by two transformation matrix ${}^C T_W$ and ${}^I T_C$ as shown figure 2.

${}^C T_W$ deals with the extrinsic parameters which express the relationship between the world co-ordinate system W and the camera co-ordinate system C , see equation (1). Furthermore, ${}^I T_C$ models the intrinsic parameters which express the optical characteristics of the camera. That is, the projection of the focal point O_C on the image plane (u_0, v_0) and the (α_u, α_v) parameters which permits to transform from the camera co-ordinate system in millimetres to the image co-ordinate system in pixels, see equation (2). The camera model determines a relationship between the 3D object point P and its 2D image point projection p by equation (3). Then, at least five couples of 2D and 3D points are needed to computed the 10 unknowns corresponding to the intrinsic and extrinsic camera parameters.

The more points we used to calibrate the camera the more accuracy we will obtained. However, we have also to take care on measuring accurately the 3D object points of the calibrating pattern and their 2D image points.

2.3 Laser Model and Calibration

In the same way of the camera modelling we have to express the relationship between the laser plane spatial characteristics and the world co-ordinate system.

Then, a laser co-ordinate system L is defined where X_L is along the direction of the laser emitter and Z_L defines the direction of the laser slit, shown in figure 5. Actually, the orthogonal vector Vd which defines the plane is only defined along Y_L obtaining that $Vd = (0, 1, 0, 0)^T$. However, the laser plane can be rotated with respect to Z_L obtaining that the orthogonal vector depending on the rotation is obtained by the equation (6). Moreover, $Vd(\alpha)$ has to be expressed with respect to the world co-ordinate system. Then, the ${}^W T_L$ matrix which express the laser co-ordinate system L with respect to the world co-ordinate system W has to be included in the model.

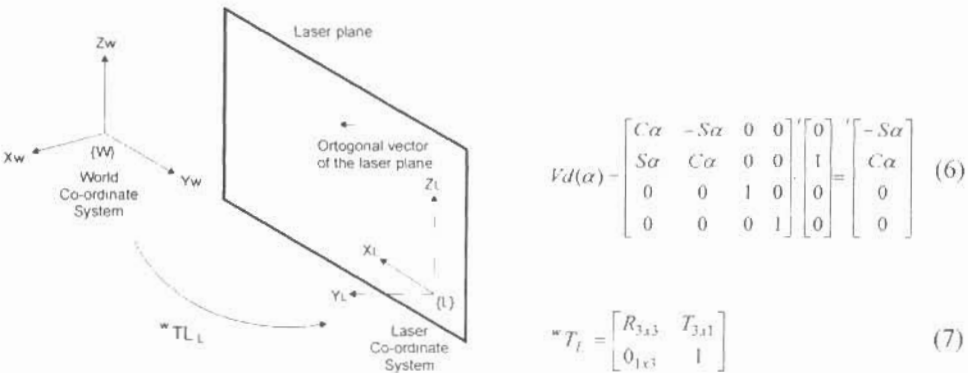


Figure 5 The laser beam model.

The ${}^W T_L$ matrix is obtained in calibration by measuring the translation and orientation of the laser co-ordinate system with respect the world co-ordinate system. This measurement is easily obtained placing the system upon a metrical floor.

3 3D Reconstruction

With the aim of dealing with the scene reconstruction we have to know the α angular position of the laser plane and get an image of the illuminated points by the laser on the scene, shown in figure 6. Firstly, we have to compute the optical ray v which goes from the focal point O_C and pass through the 2D image point $p = ({}^1 X_i, {}^1 Y_i)$ and the 3D $P = ({}^W X_i, {}^W Y_i, {}^W Z_i)$ we want to the determine, see figure 7. In order to obtain v we will fixed one of the three unknowns of P getting two 3D points P_0 and P_1 as shown in equations (8), where ${}^L T_W = {}^L T_C {}^C T_W$. Each equation determines a system of two equations and two unknowns which allow us to obtain P_0 and P_1 . Once both 3D points are known, the optical ray can be obtained from equation (9).

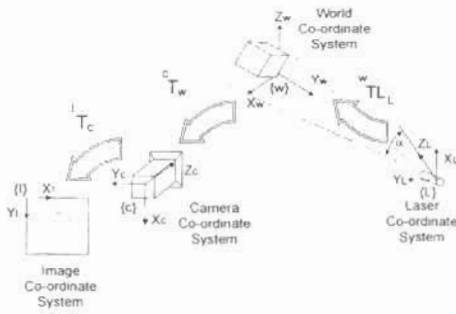


Figure 6 The 3D reconstruction principle.

$$\begin{bmatrix} s_1 \\ s_1 \\ s_1 \\ s_1 \end{bmatrix} \begin{bmatrix} X \\ Y \\ Z \\ I \end{bmatrix} = {}^I T_W \begin{bmatrix} X_0 \\ Y_0 \\ Z_0 \\ I \end{bmatrix} ; \begin{bmatrix} s_2 \\ s_2 \\ s_2 \\ s_2 \end{bmatrix} \begin{bmatrix} X \\ Y \\ Z \\ I \end{bmatrix} = {}^I T_W \begin{bmatrix} X_1 \\ Y_1 \\ Z_1 \\ I \end{bmatrix} \quad (8)$$

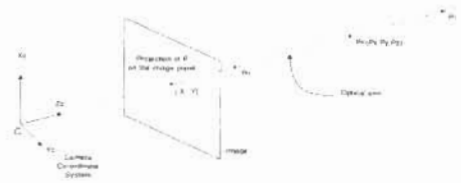


Figure 7 Obtaining the optical ray.

$$v = \frac{P_1 - P_0}{\|P_1 - P_0\|} \quad (9)$$

Then, we have to determine the intersection of the optical ray v with the laser plane in order to obtain the desired 3D point P , see figure 8. The laser plane is defined by its orthogonal vector $n = {}^W V d(\alpha)$ and a known 3D point on the plane P'_0 like for instance the origin of the laser co-ordinate system L expressed with respect to the world co-ordinate system. Moreover, we have to know the optical ray v and a point on the optical ray like for instance the already computed P_0 . Then, the desired 3D point P can be computed by using both equation of a line and a plane. The procedure is shown in equations (10).

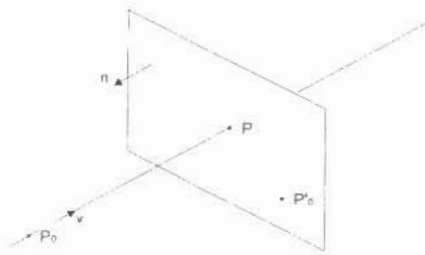


Figure 8 The principle to get the 3D object point.

$$\left. \begin{aligned} P &= P_0 + \lambda v \\ (P - P'_0) \cdot n &= 0 \end{aligned} \right\} \quad (10)$$

$$(P_0 + \lambda v) \cdot n - P'_0 \cdot n = 0$$

$$\lambda = \frac{-P'_0 \cdot n + P_0 \cdot n}{v \cdot n}$$

$$P = P_0 + \lambda v$$

4 Sensor Structure and Control

The sensor structure has been built up taking care that it has to be allocated inside the underwater robot GARBI (Amat et al. 1999). Then, a PVC structure has been constructed which allows to fixed the camera at one end, and the rotating laser at the other. The structure can be easily installed and removed from the robot, shown in figure 9 and 10.

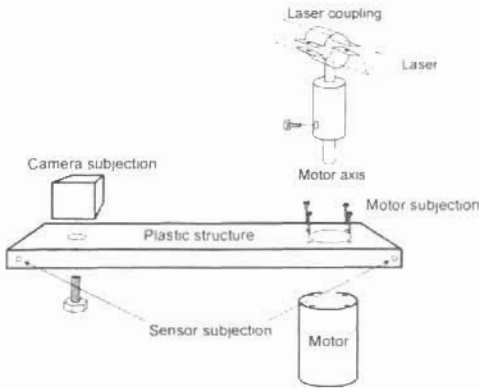


Figure 9 The structure of the system.

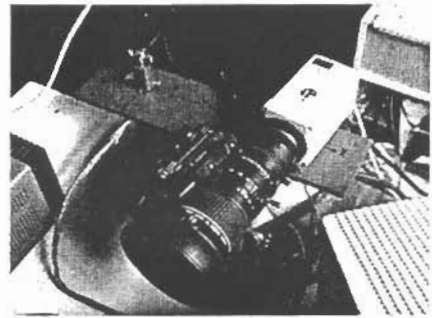


Figure 10 A detail of the sensor.

A Maxtor DC motor has been coupled with the laser emitter. Furthermore, the motor includes an incremental encoder which is used to compute the angular position of the laser plane by using a quadrature decoder. In order to establish an absolute origin of the angular position an optical barrier has been set with in the motor axis. The motor is driven by Pulse With Modulation and has been controlled by using FPGA technology and VHDL language.

4.1 Image Processing

In order to deal with the segmentation and processing of the acquired image we have used the Magtrak card developed in our lab. This card offers the possibility to process RGB images at video rate, i.e. 50 images per second. The card transforms the image from RGB to HLS and some LUTs memories are used to define the Hue, Luminance and Saturation ranges which defines the desired colour to be segmented. Once the image is segmented, the laser segments have to be thinned with the aim of obtaining the most accurate 2D positions. The thinning algorithm we have implemented in the Magtrak card computes the gravity centre of each row (note that not more than one segment can be presented in each image row). The gravity centre is obtained by computing the average of all the pixels of the same image row. The Magtrak card process each image at video rate. In parallel the Magtrak card gets the angular position of the laser synchronising it with the image capturing. Then, the gravity centres of each image row and the angular position of the laser is sent to the Computer in order to obtain the 3D reconstruction of the scene. The Magtrak card allows us to process a second image while it is sending the information of the previous to the computer, permitting to scan the whole scene without losing frames.

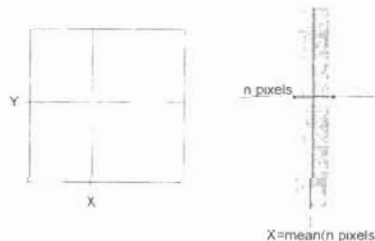


Figure 11 A segmented laser slit.

5 System Validation

Once the system is set and calibrated, we have to validate it with the aim of getting it accuracy, i.e. the discrepancy between the real 3D points and the measured ones. This section deals with the validation of the camera model and, secondly, with the validation of the laser model.

5.1 Camera Model Validation

In order to validate the camera accuracy independently of the accuracy of the laser emitter, we have to get a 2D image point of a 3D object point fixing at least one component of that 3D point of equation (11), otherwise we will have more unknowns than equations.

$$\begin{bmatrix} s_1 & {}^I X \\ s_1 & {}^I Y \\ s_i & \end{bmatrix} = {}^I T_W \begin{bmatrix} {}^W X \\ {}^W Y \\ {}^W Z \\ 1 \end{bmatrix} \quad (11)$$

Then, we have acquired one image of the calibrating pattern. Two 3D points corresponding to the plane ${}^W X=0$ and ${}^W Y=0$ and their 2D projections have been used, see figure 12. Then, the system has 2 equations and 2 unknowns and we can measure the accuracy of the camera assuming that one component is known and fixed i.e. assuming that the 3D point lies on one of both calibrating pattern planes.

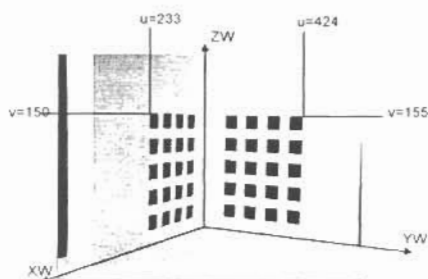


Figure 12 The 3D measured points showing their components in the image plane.

Table 1 The 2D image points, 3D real points and reconstructed points obtained.

2D Image Point	(424, 155)	(233, 150)
3D Real Point	(0, 50, 0000, 261, 0000)	(232, 0000, 0, 261, 0000)
3D Measured Point	(0, 50, 8086, 260, 6320)	(230, 6662, 0, 259, 6941)

As it is shown in table 1, we can see that the discrepancy is larger in the ${}^W Y=0$ plane than the ${}^W X=0$ because of orientation of both planes. Note that the angle between the orthogonal vector of the image plane IT and the orthogonal vector of the plane ${}^W Y=0$ is larger than with respect to ${}^W X=0$ plane.

6 Laser Model Validation

In order to validate the laser model we have to determine a) the accuracy of the angle origin ($\alpha=0$) which deals with the orientation of the laser co-ordinate system and the optical barrier used to fix the origin; and b) the accuracy of a given α which deals with the discrepancy between the real angle and the angular position measured by the encoder.

With the aim of measuring the accuracy of the angle origin, we have located the laser emitter at the origin (optical barrier activated) and the laser plane has been projected onto an orthogonal plane with respect to X_L . Furthermore, we have located a reference plane parallel to the plane $X_L Z_L$. Then, d_1 is the distance between the origin of the laser co-ordinate system L and the parallel plane, and d_2 is the distance between the projected laser slit on the orthogonal plane and the parallel plane, as show the following figure.

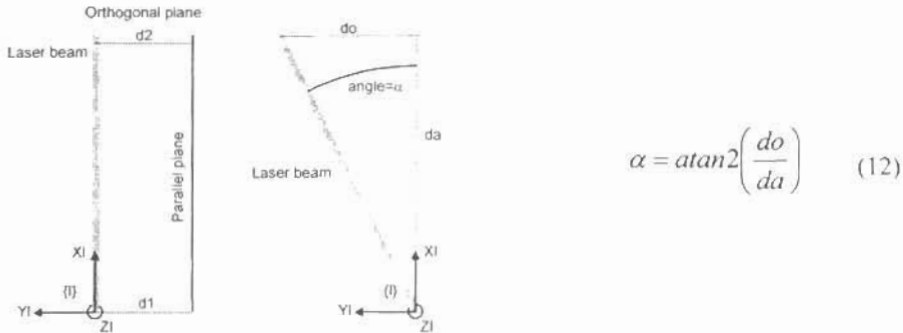


Figure 13 Both principles used for laser validation.

The accuracy of a given α is measured by moving the laser emitter to a given angle projecting the laser plane onto the orthogonal plane with respect to X_L and measuring the distances d_a and d_θ . The real angle position is obtained by the equation (12) and the measured angle is obtained by reading the encoder. The following table show the obtained results and the accuracy of the laser beam.

$d_1 \approx d_2 \approx 82$ mm.	Encoder position: 5.0°
d_θ : 2108mm	Real angle (equation 12): 5.213°
d_a : 193 mm.	Error: 0.236%

7 Experimental Results

This section shows the obtained results measuring real scenes. Example 1 deals with the accuracy of the system in flat surfaces reconstruction. The laser beam is projected on to the metrical paper stuck on the calibrating plane with an angular position of 10° . Then the laser slit is measured obtaining a line nearly parallel to Z_L , $X_L = 92$ mm, and the Y_L component is supposed to be null. Figure 14a, shows the real image, 14b, the segment image obtained by the Magtrak card before thinning and 14c the information sent by the Magtrak card to the Computer i.e. the measured gravity centre of figure 14b. Note that it appears some noise in the measures due to segmentation. Figure 14d shows the reconstructed plane obtaining a vertical plane (parallel to Z_L) where X_L is close to 105 mm, and Y_L close to 17 mm. Obtaining and error of about 1 cm, mainly due to the unevenness of the metrical paper which as it can be appreciated in the figure 14a is not properly stuck.

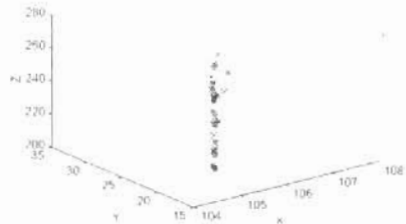
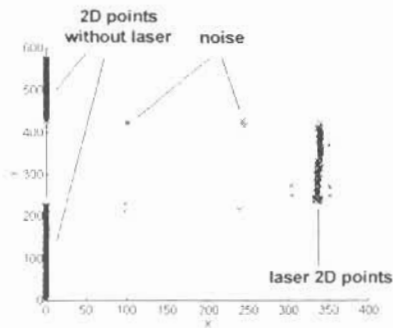
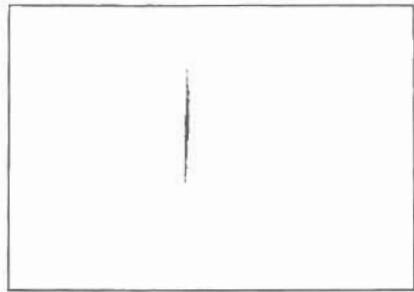
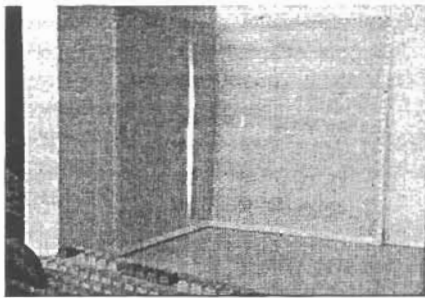


Figure 14 Example 1: a) the real scene, b) the segmented slit, c) the obtained 2D gravity centres, and d) the reconstructed slit.

The second example deals with the reconstruction of complex scenes such as a scene composed by a cylinder and a box. This example will be useful to determine if the shapes of the objects are preserved even if there exists an error in location. Figure 15a shows the real scene, the reconstruction of the scene obtained by the Computer is shown in figure 15b. Then, the reconstruction is properly oriented parallel to Y_L and a cylinder and a box are superposed to the reconstruction results in figure 15c, with the aim of enhancing the shape errors. Although it can be seen that the measures are quite accurate, the noise increase in importance measuring vanishing surfaces.

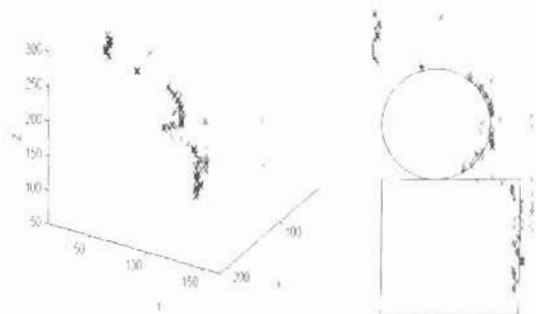
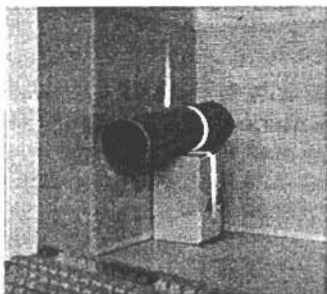


Figure 15 Example 2: a) the illuminated scene, b) the reconstructed scene, and c) a detail of the reconstructed scene with the cylinder and the box.

8 Conclusions and Further Work

A 3D reconstruction sensor has been presented. The system is based on the relationship between a single camera and a scanning laser beam. The camera model has been studied and validated obtaining a 3D location error of about 10 mm. at 2 meters. The laser emitter has been coupled to a DC Motor and an incremental encoder has been used to get its angular position. The laser model has been validated obtaining a discrepancy between the real angle and the measured one of about 3%. The image is grabbed by using a 3CCD RGB Sony camera into a specially developed card, which deals with image processing. The card segments the laser beam by using Hue and Saturation components and computes the 2D gravity centre of each image row by using an algorithm of thinning, sending this information to the computer. The computer gets the 2D points and the angular position of the encoder computing the 3D reconstruction of the scene. The paper shows some experimental results measuring a flat plane and a scene composed by a cylinder and a box.

However, the system has to be improved in the following aspects. Firstly, we have to reduce the noise that appears due to segmentation weakness as a result of light variation and so on by implementing some filtering before computing the gravity centre dealing with the removing of isolated image points. Secondly, the laser model has to be calibrated analytically in order to compute its parameters with more accuracy.

The 3D sensor can be used for several industrial applications. Moreover, the system is useful for robotic applications like indoor/outdoor navigation. In this way, we are working on adapting the system to measure undersea scenes with the aim of improving our underwater robot capabilities. However, we have to consider that the projected light will change as a result of the intrinsic colour of the objects and that the segmentation noise will increase due to scattering and the light behaviour in underwater applications.

9 References

- J. AMAT, A. MONFERRER, J. BATLLE, J. SALVI. *Cooperative Control of Two Underwater Robots*. IFAC World Congress. Invited Contribution in Marine Applications Sesion. Beijing (China). 1999. (to be published)
- S.T. BARNARD AND M.A. FISCHLER. 1982. *Computational Stereo*. International Journal on Computing Surveys, Vol. 14, No. 4, pp 553-572.
- P.J. BESL. 1988. *Active. Optical Range Imaging Sensors*. International Journal on Computing Surveys. Vol. 1, pp 127-152.
- J. S. JAFFE. 1990. *Computer Modelling and the Design of Optimal Underwater Imaging Systems*. IEEE Journal of Oceanic Engineering, Vol. 15, No. 2, pp 101-111.
- R. A. JARVIS. 1983. *A Perspective on Range Finding Techniques for Computer Vision*. IEEE Transactions on Pattern Analysis and Machine Intelligence, Vol. 5, No. 2, pp 122-139.
- J. SALVI. 1997. *An Approach to Coded Structured Light to Obtain Three Dimensional Information*. PhD. Thesis, University of Girona, Spain.